ACS APPLIED MATERIALS & INTERFACES

Evidence That Sharp Interfaces Suppress Recombination in Thick Organic Solar Cells

Obaid Alqahtani, Seyed Mehrdad Hosseini, Thomas Ferron, Victor Murcia, Terry McAfee, Kevin Vixie, Fei Huang, Ardalan Armin, Safa Shoaee, and Brian A. Collins*

Cite This: https://doi.org/10.1021/acsami.1c15570 Read Online

ABSTRACT: Commercialization and scale-up of organic solar cells (OSCs) using industrial solution printing require maintaining maximum performance at active-layer thicknesses >400 nm—a characteristic still not generally achieved in non-fullerene acceptor OSCs. NT812/PC71BM is a rare system, whose performance increases up to these thicknesses due to highly suppressed charge recombination relative to the classic Langevin model. The suppression in this system, however, uniquely depends on device processing, pointing toward the role of nanomorphology. We investigate the morphological origins of this suppressed recombination by combining results from a suite of X-ray techniques. We are surprised to find that while all investigated devices are composed of pure, similarly aggregated nanodomains, Langevin reduction factors can still be tuned from ~2 to >1000. This indicates that pure aggregated phases are insufficient for non-Langevin (reduced) recombination. Instead, we find that large well-ordered conduits and, in particular, sharp interfaces between domains appear to help to keep opposite charges separated and percolation pathways clear for enhanced charge collection in thick active layers. To our knowledge, this is the first quantitative study to isolate the donor/acceptor interfacial width correlated with non-Langevin charge recombination. This new structure−property relationship will be key to successful commercialization of printed OSCs at scale.

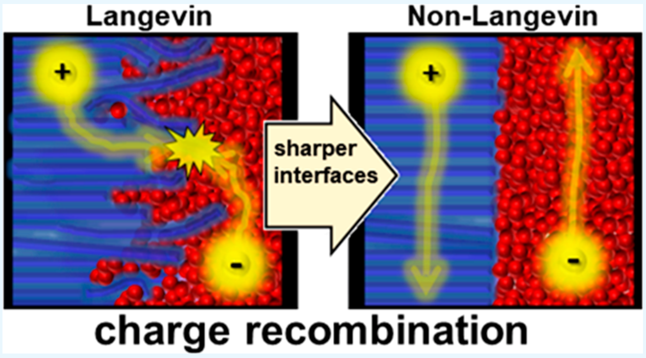

KEYWORDS: *thick organic solar cells, non-Langevin charge recombination, nanomorphology, donor−acceptor interface, resonant soft X-ray scattering (RSoXS), scanning transmission X-ray microscopy (STXM), grazing-incidence wide-angle X-ray scattering (GIWAXS)*

1. INTRODUCTION

Organic solar cells (OSCs) with solution-printed active layers have attracted a great deal of attention due to their tunable properties, mechanical flexibility, and continuously rising power conversion efficiency (PCE) in the last 2 decades.[1,2] The current PCE record for OSCs is about 18%.[3,4] In bulk heterojunction (BHJ) OSCs, where electron-donating and -accepting materials are blended together in a common ink, the PCE usually maximizes when the thickness of the active layer is around 100 nm. As the BHJ thickness increases, the light absorbance increases following an interference-induced oscillatory pattern, potentially resulting in higher current densities in the thicker junctions. However, charge recombination increases faster with increasing thickness, scaling inversely with the square of the film thickness.[5] Consequently, in most polymer-based OSCs, the device performance rapidly decreases as the BHJ thickness increases beyond the first absorbance interference peak.[6−9] One of the existing challenges facing the industrialization of OSCs at a large scale is the difficulty of controlling and processing thin active layers.[10] This is because most large-scale fabrication methods, for example, roll-to-roll printing, can only reproducibly deposit pinhole-free films greater than 400 nm.[11]

The investigated system is among the relatively few systems that maintain high efficiencies in the thick junction regime.[10,12] The recently synthesized electron-donating copolymer, Naphtho[1,2-*c*:5,6-*c*′]bis([1,2,5]thiadiazole)-based copolymer (NT812, Figure 1a bottom), exhibits PCE > 10% when fabricated into OSCs with phenyl-C71-butyric acid methyl ester (PC71BM) fullerene as the electron acceptor (Figure 1a top).[13] The novelty of NT812 appeared when this system maintained a high PCE even with thick BHJ active layers ~1 μm. It was found that under optimal fabrication conditions,

Received: August 15, 2021
Accepted: November 1, 2021

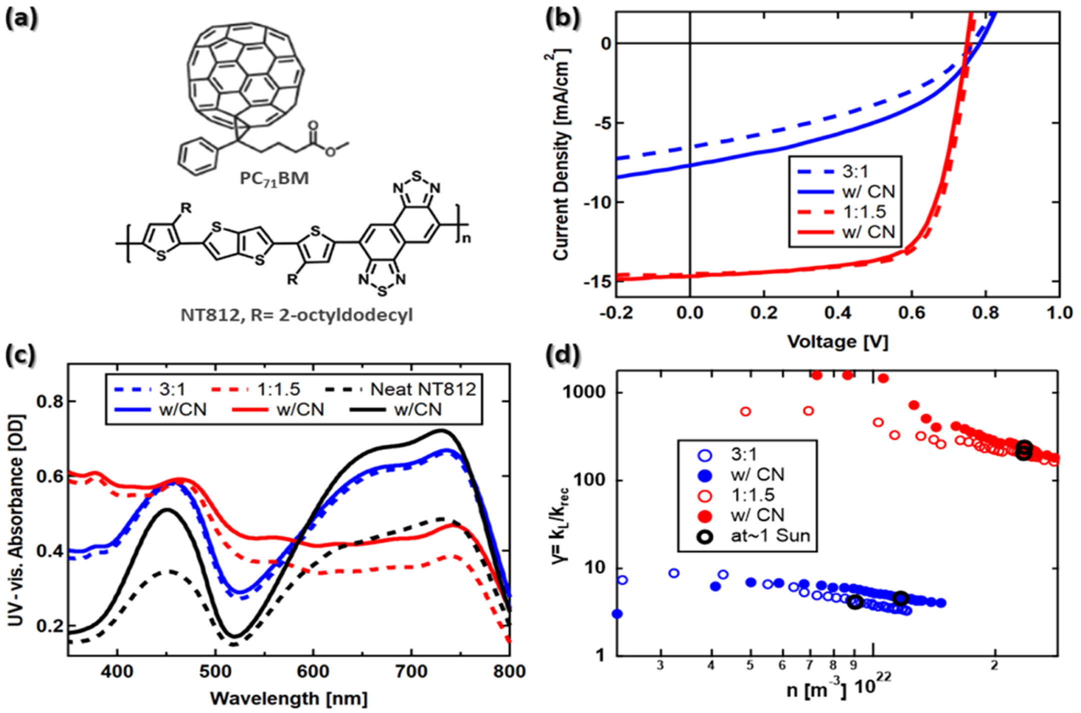

Figure 1. (a) Chemical structure of the fullerene (top) and polymer (bottom). (b) *J*−*V* characteristic curves of the four different solar cells. (c) UV−vis absorbance spectra of a neat polymer with and without CN as well as for all blends. (d) Reduction factor of bimolecular recombination as a function of carrier density in all four NT812/PC71BM blends. Black circles show the reduction factor data points at about 1 sun.

bimolecular recombination is significantly suppressed up to 800× below what is expected for the diffusive Langevin model (where charges' trajectories are random and depend on the charge carrier mobilities—for more details, we refer the reader to our previous work[7] or to the original work of the Langevin classical model[14]). This non-Langevin behavior leads to OSCs with less recombination losses, that is, Shockley-type solar cells.[7] In fact, recombination is suppressed so much in these systems that their performance increases rather than decreasing with thicknesses of up to 300 nm, making them one of the highest-performing systems to exhibit such favorable behavior.[15] Although non-fullerene acceptor (NFA) systems dominate performance with thin active layers, work to reduce recombination in these systems has only just begun,[16] and to our knowledge, no NFA systems have demonstrated such increased performance beyond the first interference maximum.

Investigation into the origin of this phenomenon demonstrated that the charge mobilities of the NT812/PC71BM system are rather mundane and cannot explain the very efficient charge collection. A proposed scenario is either a unique interfacial charge transfer (CT) state with fast dissociation dynamics relative to the decay rate or a special morphology that allows thick non-Langevin BHJ OSCs.[7,17] A combinatory scenario can be possible as well where improved nanomorphology enhances CT state dynamics. Importantly, one study found that nearly classical Langevin recombination could be achieved in this system by changing the donor−acceptor ratio,[7] which indicates a morphological origin to the non-Langevin behavior. Only a handful of other D/A combinations show similar behavior.[9,18,19]

General work on the topic has suggested that the high crystallinity of the donor is important[20,21] or in the case of amorphous polymers, that relatively pure phases help by reducing charge recombination.[22] Unfortunately, early experimental and computational work investigating interfacial sharpness on recombination has resulted in conflicting conclusions. While some reports suggest that sharp interfaces reduce recombination,[23,24] others conclude that disordered or mixed interfaces are best.[25,26] However, none of these studies directly measured BHJ interfacial properties such as interfacial sharpness. Clarke et al. compared two polymer/fullerene systems with similar nanostructures but distinct charge recombination behaviors to probe the morphological origins of non-Langevin dynamics. Their transmission electron microscopy (TEM) investigation could not reveal any significant morphological difference, however, and they were not able to compare Langevin and non-Langevin recombination in the same material system.[27] The NT812/PC71BM system, with its ability to switch between the two behaviors, represents an opportunity to reveal the critical nanostructure leading to non-Langevin recombination but will require an advanced quantitative characterization of the nanostructure.

We have shown in our previous work that the critical morphological parameters of crystallinity, domain purity, and domain size can be measured by a strategic application of a suite of synchrotron X-ray techniques.[28−30] Our recent work has demonstrated the capability of these techniques to additionally probe interfacial sharpness.[30,31] The work highlighted the importance of interfaces on charge generation but was not conclusive with respect to recombination. Venkatesan et al. noted reduced recombination with enhanced Kelvin probe surface potential differences between domains in blends cast from solvent additives.[32] This correlated with increased domain purity, but they did not investigate interface morphology. Another study reported evidence that rough D/A bulk heterointerfaces correlated with good exciton dissociation but did not monitor recombination.[33] Thus, to date, no work has directly measured morphology, including

Table 1. Summary of Device Performance, Reduction Factors of Bimolecular Recombination, and Charge Carrier Mobilities in NT812/PC71BM Films with Different Blend Ratios, Processed with and Without a Solvent Additive

blend(NT812/PC71BM)	additive CN [vol %]	V_{OC} [V]	J_{SC} [mA·cm^{-2}]	FF [%]	avg. PCE [%]	$\gamma = k_L/k_{rec}$	μ_s [cm^2 V^{-1} s^{-1}]	μ_f [cm^2 V^{-1} s^{-1}]
(3:1)	0	0.77	6.42	39	1.88(0.08)	2	2.5×10^{-4}	2.5×10^{-4}
(3:1)	0.5	0.78	7.49	41	2.43(0.06)	5	3.0×10^{-4}	3.0×10^{-4}
(1:1.5)	0	0.75	14.69	70	7.85(0.25)	200	2.2×10^{-4}	8.1×10^{-3}
(1:1.5)	0.5	0.74	14.79	69	7.67(0.13)	250	2.9×10^{-4}	9.0×10^{-3}

The device performance parameters are the average of six devices. The bimolecular recombination reduction factors ($\gamma = k_L/k_{rec}$) are calculated based on steady-state bias-assisted charge extraction measurements and the mobilities (fast and slow carriers) are calculated based on resistance-dependent photovoltage measurements (see Figures S2 and S3, Supporting Information). The listed γ values are at about 1 sun intensity.

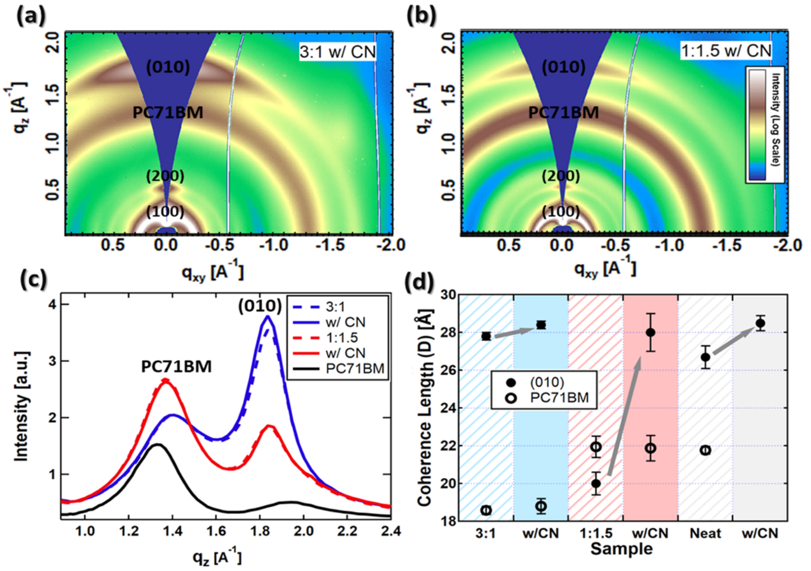

Figure 2. GIWAXS results of neat materials (NT812 and fullerene) and blends. 2D GIWAXS scattering results of NT812: PC71BM blends of the (3:1) blend with CN (a) and 1:1.5 blend with CN (b). The 2D images are plotted with the same color scale of the scattering intensities [au], also corrected for the missing wedge. (c) 1D GIWAXS profiles extracted from the 2D images in the OoP vertical direction (q_z) for all blends. Also, the graph includes the GIWAXS profile of neat PC71BM (black) to help with peak assignments. PC71BM and (010) peaks are indicated in the graph. (d) Coherence length (D) of the PC71BM peak at q_z = 1.36 Å^{-1} (open circles) and (010) peak at q_z = 1.83 Å^{-1} (solid circles) in blends as well as in neat materials calculated via Scherrer analysis (details in the Supporting Information).

interfaces, while at the same time isolating and suppressing recombination.

In this work, we apply our suite of X-ray nanoprobes to directly reveal the critical morphology behind the activation of highly suppressed non-Langevin recombination. We uniquely combine our measurements to quantify the donor−acceptor (D−A) interfacial sharpness in BHJ blends. Varying the active layer blend ratio and solvent additive content effectively switches the charge recombination dynamics between Langevin and non-Langevin in the same system, suggesting that reduced recombination is morphology-driven. We are surprised to find that even our active layers exhibiting Langevin recombination are composed of pure, well-aggregated phases. Instead, we find that large domains with sharp D−A interfaces correlate with suppressed, non-Langevin recombination with reduction factors >1000, indicating that these are the morphological mechanisms that enable thick and efficient active layers. Such findings can guide future research to achieve high-preforming systems suitable for the large-scale production of OSCs.

2. RESULTS

OSC active layers were spin-coated with (D/A) blend wt. ratios of (1:1.5) and (3:1) both with and without 0.5 vol % chloronaphthalene (CN) as a solvent additive since these conditions exhibited both Langevin and non-Langevin recombination dynamics previously.[7] Rather than 1 μm thick active layers, ∼200 nm active layers were investigated to enable both device physics and X-ray nanoprobe analyses on the same set of samples by the participating groups. 100 and 200 nm active layers revealed identical morphologies and performance scaled only by absorption (see Figures S1, S26 and S27, Supporting Information). It is worth noting that our previous device physics investigation of thin (100 nm) and thick (800 nm) films shows similar carrier mobilities in both junctions.[7] Thus, thicker films are likely to have similar morphologies. Figure 1b displays the J−V curves under AM 1.5 G solar illumination, and Table 1 summarizes device performance metrics which are similar to previous reports.[7,13] In particular, the (1:1.5) devices show about 4 times more efficiency than (3:1) blends with all of the improvement from the short-circuit current (J_{sc}) and fill factor (FF).[34] Although UV−vis spectra of pure films show some differences when adding the CN additive, no significant difference in aggregation due to CN can be detected in the blends investigated, suggesting that the polymer in all blends is well aggregated.

Figure 1d shows the reduction factor of the bimolecular recombination γ, which is the ratio of the classical Langevin recombination coefficient k_L[14] to the coefficient k_{rec} in a given photoactive layer, $\gamma = k_L/k_{rec}$. The bimolecular recombination in the limit of a homogeneous medium can be approximated by the Langevin recombination rate constant, which is proportional to the mean carrier mobility. This was calculated in a similar manner to our previous work (see Figure S2, Supporting Information).[7] As expected, the (3:1) blend without the CN additive exhibits nearly classical diffusive Langevin recombination. In contrast, the (1:1.5) devices show about 2 orders of magnitude lower recombination coefficients with $\gamma_{max} > 1000$. The (1:1.5) devices are, therefore, considered to exhibit non-Langevin recombination dynamics. The solvent additive also improves the reduction factor (more significantly for the 3:1 blends) with all trends holding true under the operational conditions (∼1 sun), see Table1 and the black circles in Figure 1d.

Resistance-dependent photovoltage (RPV) transient measurements were used to separately determine faster and slower carrier mobilities in each blend. All mobilities are unremarkable and rather typical of values in other high-performing polymer/fullerene OSCs—in agreement with previous work.[7] We were not able to separate the slower and faster carrier mobilities in the (3:1) blends, likely due to them being too similar. Importantly, there are no significant changes in mobilities due to processing conditions other than the fast carriers (typically identified as electrons in the fullerene phase)[35,36] having increasing mobilities in the films with the better blend ratio as shown in Table 1 (also see Figure S3, Supporting Information). However, increasing electron mobilities only serve to unbalance the charge transport, and even these mobilities are still typical of polymer/fullerene blends. These results suggest that the charge extraction rate is not extraordinary, but rather the bimolecular recombination rate is low. This allows for efficient charge collection even when the film thickness increases.[7] Contrary to mobility, γ improves by about 100 times with the blend ratio. In many other OSCs with either polymer or small molecule donors, the non-Langevin behavior has been shown to be key for maintaining a high FF even at an active layer thickness ∼300 nm.[9,17,18,37,38] Thus, the lower FF values in (3:1) blends can be attributed to their higher biomolecular recombination in comparison to their (1:1.5) counterparts.

We now turn to morphological characterization to understand how the additive and D−A ratios can turn on and off the Langevin recombination property. We first investigate the crystallinity of the electron donor (NT812) and fullerene (acceptor) aggregates using grazing-incidence wide-angle X-ray scattering (GIWAXS) measurements. The results of the experiments on both neat and blend films are presented in Figure 2 with additional results and analysis provided in the Supporting Information. Figures 2a,b shows 2D GIWAXS images of (3:1) and (1:1.5) blends, respectively, both with CN. The strong scattering ring at q = 1.36 Å^{-1} indicates the presence of pure PC71BM aggregates as evidenced by the similar ring for a pure PC71BM film. The scattering peaks at q = 0.29 Å^{-1} indicate polymer lamellar (100) stacking with only a weak second-order (200) peak detectable. The primarily out-of-plane (OoP) peaks at q_z = 1.83 Å^{-1} represent π-stacking (010) with a face-on orientated population with respect to the substrate in addition to a randomly oriented crystal population. We focus on these face-on π-stacking peaks because this packing is favorable for charge transport. Figure 2c shows 1D GIWAXS profiles extracted from the 2D images in the OoP direction, that is, a line cut in the vertical direction (q_z). Figures S5 and S7, in the Supporting Information, show vertical and horizontal 1D profiles and peak assignments. The intensities of both peaks closely follow the blend ratio, suggesting that the degree of crystallinity or aggregation is similar in all blends. Pole figure analysis of (010) supports the claim of similarity in the degree of crystallinity in all blends (see Figure S9, Supporting Information). The polymer and PC71BM diffraction characteristics in all blends are consistent with those of their pure film counterparts and suggest the existence of both pure polymer and pure PC71BM domains in all active layers.

Results of peak width Scherrer analysis (Figure S6, Supporting Information) of the coherence length (D) are displayed in Figures 2d and S8, Supporting Information—where D is a measure of length-scale ordering within a crystal or crystal size.[39] In each case, the solvent additive enhances ordering in the blends by increasing D for the OoP π-stacking (Figure 2d). While there is little change in π-stacking for the (3:1) blend film, π-stacking is significantly enhanced for the (1:1.5) blends. A similar improvement occurs for electronically insulating lamellar stacking (Figure S8, Supporting Information). All blends cast with the CN additive, however, have similar π-stacking coherence lengths to that of the pure polymer film. The enhancement of the coherence length with CN is consistent with its role as a plasticizer and the effect of the fullerene to increasingly disrupt polymer packing.[40] In contrast to the polymer packing, the D of the main fullerene peaks are invariant with CN, and D values in (1:1.5) blends are equal to those in pure fullerene. (3:1) blends show similar but smaller values of fullerene D. This suggests slightly more disordered PC71BM aggregates in (3:1) films, which are consistent with lower electron mobilities in these blends as interpreted from our RPV experiments. The coherence length also sets a lower limit to the size of pure phases in the blends. We cannot say much about the size of pure fullerene domains as even pure films only exhibit diffraction with D ∼ 2 nm (Figure 2d). However, the polymer lamellar diffraction demonstrates D ∼ 14 nm for all samples (Figure S8, Supporting Information), making this the lower limit of pure polymer domains in the blends. From Figure S8, it is noticeable that the D of the lamellar peak in neat polymer films is lower than those in the blends. Although this might seem counterintuitive, there is a precedent in the literature for other systems that show similar behavior.[41] We observe that as the amount of fullerene increases, the in-plane lamellar peaks narrow and thus result in a higher coherence length (Figure S8). Such an effect could arise from a strong drive to phase separate early during film formation, enabling more time to order.

To more accurately probe domain size, composition, and connectivity, we used scanning transmission X-ray microscopy (STXM)[42] combined with near-edge X-ray absorbance fine structure (NEXAFS) spectroscopy.[43] Figure 3 presents NEXAFS and STXM results of a (1:1.5) with a CN blend with film thickness ≈100 nm for better clarity in the transmission-mode image. The similarity of the results on this film was confirmed by identical scattering profiles between the thinner and thicker active layers (see Figure S26, Supporting Information) as well as qualitative STXM images of thicker films (Figure S16, Supporting Information). The linear fitting of NEXAFS spectra for the blend, shown in Figure 3a, confirms the average weight ratio, 40% polymer, across the film. Figure 3b presents a STXM image where dark regions

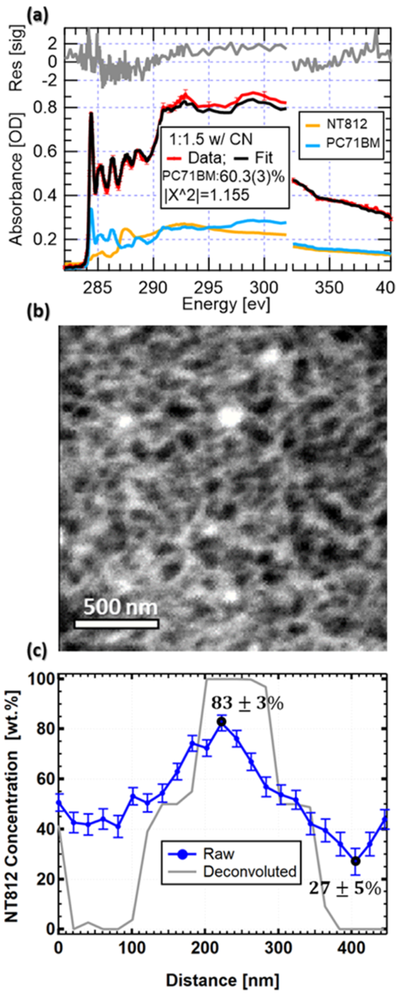

Figure 3. Morphology investigation of the OSC active layer in a 100 nm thin (1:1.5) blend with CN. (a) NEXAFS spectra: pure NT812 (orange), PC71BM (blue), blend (red), and a linear combination fit of spectra for NEXAFS of pure components (black). (b) STXM composition scan acquired at 284.4 eV, which is the fullerene absorption peak. PC71BM (dark regions) and NT812 (white fibrils). (c) Concentration profiles of NT812 across different compositional domains: (blue) raw and (gray) deconvoluted.

represent a matrix of (50−100 nm sized) PC71BM-rich domains and the white fibrils indicate polymer-rich domains that are 30−50 nm in width. These measurements are consistent with the lower limits of domain size determined from the GIWAXS analysis. The fibrillar nature of the polymer domains indicates well-connected pure crystalline polymer conduits for hole transport that are larger than those in the classical P3HT-based OSC fibril network. The PC71BM domains are large enough to easily connect to the electrodes—we anticipate that to hold true even in thick films. A qualitative comparison between the two blend ratios with active layers with thicknesses >200 nm (see Figure S16, Supporting Information) shows a similar fibril network with the (3:1) film exhibiting polymer fibrils with a smaller spacing due to less PC71BM loading. The spectroscopic nature of STXM imaging enables chemical mapping of the domains. Our quantitative analysis (details in Figures S12 and S13, Supporting Information) is carried out on the thinner 100 nm film in regions likely to be mostly one domain throughout the film thickness (e.g., nodes of polymer fibrils) with an example composition line profile shown in Figure 3c (many more in Figure S13, Supporting Information). The peaked nature of the composition profiles originates from the STXM beam size (∼50 nm). After correcting for the X-ray beam convolution in a similar fashion to our previous work (details in Figures S14 and S15, Supporting Information),[29] the deconvoluted results indicate pure polymer and pure fullerene domains, agreeing with the GIWAXS analysis. We were not able to conduct compositional analysis on thick films due to vertically overlapping domains.

We now turn to resonant soft X-ray scattering (RSoXS) as a complementary measurement of domain size and purity with the unique opportunity to also investigate D−A interfaces.[44] The Lorentz-corrected RSoXS scattering profiles in Figure 4a were strategically acquired just below the absorption edge to enhance phase contrast, limit damage, reduce orientation contrast, and eliminate X-ray fluorescence backgrounds. They show that the (3:1) blends have scattering peaks at q = 0.10 nm^{-1} which corresponds to a characteristic length (which determines the average center-to-center distance between scatterers and is defined as $L_C = 2\pi/q^*$, where q^* is the peak position) of 62 nm. On the other hand, the (1:1.5) films show scattering peaks at q = 0.064 nm^{-1} and $L_c \approx$ 98 nm.

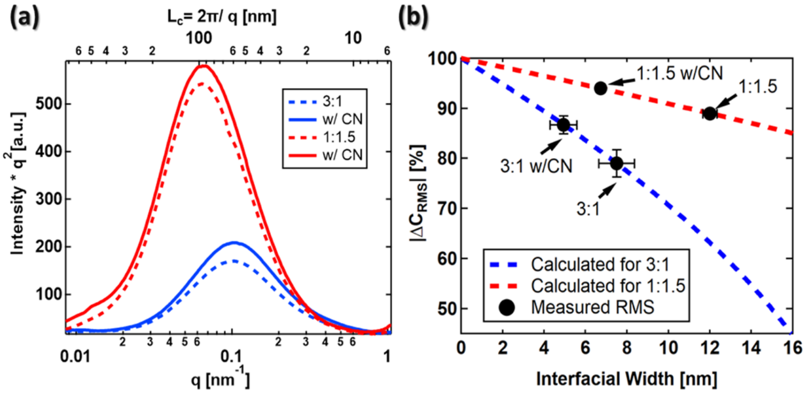

Figure 4. (a) Lorentz-corrected RSoXS profiles acquired at 283.5 eV for active layers of the four investigated samples as indicated in the graph legend. (b) Averaged differences in composition between different domains based on a two-domain model. The dotted lines represent the mathematically calculated ΔC_{RMS} values of composition differences as a function of the D−A interfacial width. The black circles are the extracted values of the D−A interfacial width based on STXM and RSoXS results.

Although without modeling these values are only approximate, however, they are consistent with the domain spacing from STXM analyses. Given that the (3:1) blends are 75% polymer, it is likely that the polymer domains in this blend are the same size as in the (1:1.5) blend. This is due to the self-limiting nature of polymer fibrils seen in most semicrystalline polymer films. Thus, a smaller characteristic length is likely due to a reduction in fullerene domain size to below 30 nm as estimated from L_C as detailed in Supporting Information, part S10. CN does not affect the peak position and therefore has no impact on the characteristic length (Figure S20, Supporting Information) but does increase the scattering intensity. The insensitivity of L_C to the plasticizing CN indicates that the nanostructure is driven by crystallinity rather than liquid−liquid phase separation. Furthermore, anisotropic scattering at the X-ray energy of 285.4 eV was measured and has been interpreted as indicating a preferential molecular orientation at D−A interfaces, similar to other systems.[45] Here, the scattering anisotropy is the same sign for all blends, suggesting that the D−A interfacial orientation does not change with the investigated processing conditions and is thus not a significant factor determining performance in this case. Additional tilted-film RSoXS measurements, conducted to express the q_z component (see Figure S22),[46] were consistent with no vertical stratification and in agreement with pure domains measured in STXM that integrates the vertical film direction.

The increase in RSoXS intensity with CN suggests that the solvent additive enhances the average composition variation between the polymer and fullerene domains. The total scattering intensity calculated by integrating the scattering profiles over all reciprocal space (area under the profiles in Figure 4a) is proportional to the mean-squared composition difference between domains ($\Delta C_{\mathrm{RMS}} \propto \sqrt{\mathrm{TSI}}$, RMS is root mean square).[29] ΔC_{RMS} was calculated on an absolute scale by combining this measurement with the STXM domain composition analysis and prior knowledge of the donor/acceptor ratio as we have done in our previous work[29] with details shown in Figures S17−S21, Supporting Information. Figure 4b displays the result of this analysis (y-axis) with uncertainties primarily from convolution of domain composition with the volume fraction (Figure S21, Supporting Information). The ΔC_{RMS} analysis tracks the RSoXS profile intensities seen in Figure 4a with the average domain composition fluctuation greatest for the (1:1.5) blends and with the CN additive.

There is significant evidence (from GIWAXS and STXM) that both polymer and fullerene domains are pure. However, $\Delta C_{\mathrm{RMS}} < 100\%$ means that mixed regions of the active layer must exist somewhere. There is no clear evidence of a separate third phase in our STXM images, so the mixed region must actually be manifest as interfacial mixing in a narrow region below the resolution limit of the microscope. Such an interpretation follows from other systems like this one where evidence of mixing with fullerenes only occurs at polymer fibril interfaces.[30,47−49] Previously, we determined the interfacial width in a block copolymer using the absolute scattering intensity.[46] The required measurements for such analysis were not conducted here, but we can instead combine ΔC_{RMS} with measurements of the domain spacing and volume fraction to extract the interfacial width. In this calculation (detailed in Figures S23−S25, Supporting Information), we assume circular fibril cross-sections and a linear interfacial composition profile. This results in a simple analytic solution for the interfacial width between pure domains, which notably makes no assumption of the packing arrangement of the fibrils and is also robust to a wide distribution of fibril sizes. The results of calculating the interfacial width are shown as the x-position of the black dots in Figure 4b. Thus, we attribute the increase of ΔC_{RMS} with the CN additive to the D−A interfaces becoming sharper, with the widest interfaces at 12 nm sharpening to less than 5 nm in width. In short, the CN plasticizing solvent additive enables cleaner crystallinity-driven phase separation, sharpening the D−A interfaces.

3. DISCUSSION

Figure 5 depicts the morphology of the investigated NT812:PC71BM active layers that is consistent with all measurement results and analysis presented above. Blue represents pure polymer fibrils in a red matrix of pure fullerene. The black bars symbolize polymer chains inside the fibrils whose packing slightly improves with the solvent additive (see coherence length measurements). Notably, there is only evidence of improvement in 1:1.5 blends but not in 3:1 blends (see also the UV−vis spectra for 3:1 blends). The color gradient at fibril edges depicts interfacial mixing which decreases with the CN additive, thus making the domain interfaces sharper (and increasing ΔC_{RMS}). Finally, more fibrils closer together are depicted for the (3:1) blend ratio making the fullerene domains smaller and reducing the characteristic length as evidenced by the RSoXS analysis.

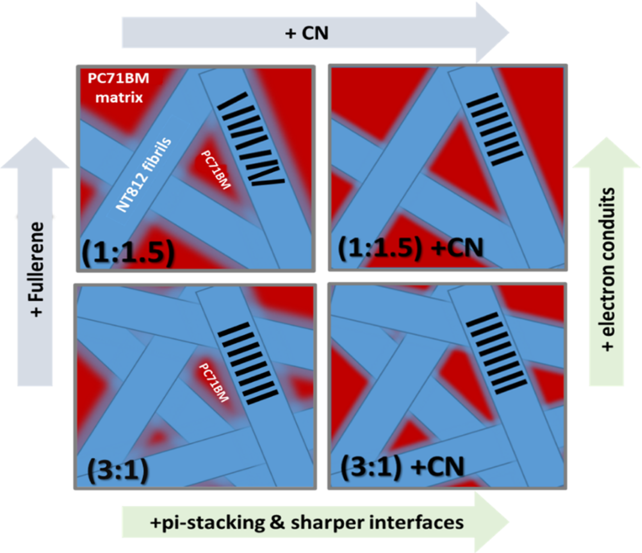

Figure 5. Depicted representation of the morphology of the OSC active layer in the investigated NT812/PC71BM blends. Polymer fibrils (blue) with stacked polymer chains (black) and the matrix of fullerene (red). We note that the fast growth direction of the fibril is unknown for this polymer and may not be the pi-stacking direction as is depicted here.

The question to be answered is what aspects of morphology are important to realize highly suppressed, non-Langevin recombination. In general, it has been found that domain purity in polymer-based OSCs is important for device performance by aiding charge extraction and hindering recombination.[22,24,50,51] This is likely an important prerequisite here, but the presence of pure domains in blends exhibiting both Langevin and non-Langevin recombination suggests that this situation alone is insufficient. Venkatesan et al. have shown that charge recombination is high in low-performing polymer/fullerene systems with narrow domains despite good domain purity and conductivity.[52] Our results go further to show that large and clean conduits to the electrodes keep charges from interacting with their counterparts in neighboring domains, whereas narrow pure domains increase the likelihood that charges will encounter each other or trap states at the interfaces. This is the most prevalent morphological change between the cells with Langevin versus non-Langevin recombination dynamics. Note that the 25% PC71BM loading in the (3:1) blends, aggregating into pure phases, is well above the 3D percolation threshold. Therefore, although isolated-domain traps are possible,[53,54] general fullerene domain connectivity should be no issue here.

A further clue to the importance of interfacial interaction comes from the correlation of sharpening interfaces rather than crystalline coherence with decreased recombination for both blend films. In particular, in (3:1) blends, the recombination reduction factor γ more than doubles when interfacial mixing is reduced through the CN additive, while there is no detectible change in crystallinity (GIWAXS) or aggregation (UV−vis spectroscopy). The improvement in γ is not nearly as significant for the corresponding (1:1.5) blend devices, even though pi-stacking improves dramatically for them. We interpret this situation to mean that highly mixed or wide D−A interfaces can encroach on the charge pathways—especially when they are narrow—and enable holes and electrons to mingle and recombine in a way well described by the Langevin model. Devices with large pure percolation pathways are more immune to interfacial details such that sharper interfaces are less critical for non-Langevin recombination.[55] The crystallinity improving with CN might also help in keeping holes toward the middle of transport conduits because the energy states in a well-delocalized crystal are lower than those in a defective crystal,[56] thus resulting in even higher γ. The domain size must not be allowed to increase too far, however, due to the limitations of the exciton diffusion length (∼20 nm). On top of suppressing recombination, there is increasing evidence that sharp interfaces are important for charge generation as well in semicrystalline systems.[30,31] Thus, the highest efficiency devices will likely still depend on sharp interfaces and smaller domains to simultaneously harvest all excitons and transport charges.

Although we cannot conclusively say that perfectly discrete (zero width) interfaces are best, we have been able to uniquely remove the effects of domain purity and crystallinity/aggregation from the equation. Furthermore, our direct correlation with the Langevin reduction factor rather than short-circuit current enables us to eliminate possible influences of changing charge generation rates. Combined, these results reveal a definitive influence of interfacial sharpness on suppressing recombination.

To put our findings about the NT812 system into perspective, we compare it to the classical electron donor, poly3-hexylthiophene (P3HT), which exhibits non-Langevin recombination as well in fullerene-based BHJ OSCs with thermal post-treatment.[38,57,58] Both systems phase segregate in BHJ layers and result in pure fibrils under optimal fabrication conditions and both have similar charge carrier mobilities. In fact, fibrillar structures are good at purifying, sharpening, and limiting how large the domains get, so they do not get so big as to lower exciton dissociation efficiencies. However, the best NT812 OSCs' γ values are higher than those for P3HT devices (>1000 vs 100 s). We attribute this to the fact that NT812, like many other polymers,[59−61] has a stiffer and longer monomer than P3HT, which causes the NT812 fibrils to be wider, resulting in larger charge conduits. On the other hand, there is significant room for improvement in NFAs which now top OSC performance in thin layers but lose significant efficiency as thickness increases, even when processed to optimize aggregation.[16] Therefore, more systems with an NT812-type morphology are needed, namely, with larger fibrils that strongly phase separate from the acceptor phase to result in sharp interfaces. Such a strategy will enable high efficiency devices with thicknesses >400 nm.

4. CONCLUSIONS

We have investigated the morphological mechanisms behind a novel high-performing polymer/fullerene OSC system known to exhibit both highly suppressed non-Langevin recombination and classical diffusive Langevin recombination dependent on the blend ratio. Our suite of synchrotron-based X-ray techniques were combined to reveal pure phases under all preparation conditions, suggesting that pure phases alone are not sufficient to realize non-Langevin recombination. Instead, we found that larger (>30 nm), pure, and well-aggregated domains with sharp D−A interfaces likely act as charge conduits across the active layers to effectively segregate charges and suppress bimolecular recombination via fast dissociation of CT states for near-ideal charge generation and collection. Such morphological features are possible explanations to how efficient devices can be achieved with printable active layers up to 1 μm in thickness. Thus, large, pure percolation pathways with sharp heterointerfaces may be required to achieve efficient OSCs suitable for large-scale industrial production.

5. EXPERIMENTAL SECTION

5.1. Device Fabrication. The polymer (NT812) was supplied by Fei Huang of the Institute of Polymer Optoelectronic Materials and Devices, South China University of Technology. The fullerene acceptor, PC71BM, was purchased from Solenne. The solvents, chlorobenzene (CB) and 1,2-dichlorobenzene (DCB), and the additive CN were purchased from Carl Roth and Alfa Aesar, respectively. The devices were fabricated with a conventional structure. First, the patterned indium tin oxide (ITO) glass substrates were cleaned in an ultrasonic bath with detergent, acetone, deionized water, and isopropyl alcohol and dried by nitrogen. The dried substrates were treated with oxygen plasma at room temperature for 4 min. Then, PEDOT/PSS [purchased from Heraeus Deutschland (Clevios P AI4083)] was spin-coated on top of the substrates (3000 rpm for 30 s, thickness of ≈30 nm), and the substrates were annealed at 150 °C for 15 min in air. For deposition of active layers, blend solutions of NT812 and PC71BM at weight ratios of 1:1.5 and 3:1 dissolved in CB/DCB = 3:1 (with/without 0.5 vol % of CN) with a total concentration of 20 mg mL^{-1} were spin-coated on top of a PEDOT/PSS layer in a nitrogen filled glovebox. The blend films were annealed at 100 °C for 15 min on a hot plate. After cooling down, a 5 nm poly 9,9-bis(6-*N*,*N*,*N*-trimethylammonium) hexylfluorene-*alt*-co-phenylenebromide (PFN−Br) layer was spin-coated from methanol solution onto the active layers. Finally, the films were transferred into a vacuum evaporator connected to the glovebox, and 100 nm silver was deposited sequentially through a shadow mask under ≈1 × 10^{-7} mbar, with an active area of the cells of A = 0.06 cm^2.

In order to prepare the films for morphology study, silicon wafers were cleaned during the ITO substrate cleaning process, and then, Na/PSS was spin-coated (3000 rpm for 30 s) on top of it to simulate the device PEDOT/PSS surface roughness and surface energy. The substrates were annealed at 150 °C for 15 min in air. The active layers were spin-coated and then thermally annealed as described above.

5.2. Resistance-Dependent Photovoltage. The devices were illuminated by a pulsed second harmonic Nd/YAG laser (NT242, EKSPLA) at 532 nm with a 6 ns pulse duration. The laser intensity was attenuated with a normal optical density filter and set to a low intensity in order to prevent a redistribution (screening) of the internal electric field and maintaining quasi-short-circuit conditions regardless of the load resistance. Then, the photocurrent and photovoltage transients were recorded by a digital storage oscilloscope (DSO9104H) via a LabVIEW code. One should refer to previous work for more details about those techniques.[7]

5.3. Bias-Assisted Charge Extraction. To establish steady-state conditions, we used a high power (1 W, 638 nm) laser diode (InsaneWare) with a switch-off time of 10 ns. The laser diode was operated at (500 Hz) with a duty cycle of 50%, such that illumination lasted 1 ms and the diode was switched off also for 1 ms. A pulse generator (Agilent 81150A) was used to apply the prebias (V_{OC}) and collection bias which are amplified by a home-built amplifier, allowing a fast extraction time of 10−20 ns. The current transients were measured via a (10 Ω) resistor in series with the sample and recorded with an oscilloscope (Agilent DSO9104H).

5.4. Morphology Measurements. To probe the active-layer nanomorphology in the investigated OSC systems, we utilized synchrotron-based X-ray microscopy, spectroscopy, and scattering techniques. GIWAXS, RSoXS, and Spectroscopy/STXM were conducted at the Advanced Light Source, Berkeley, CA at beamlines 7.3.3,[62] 11.0.1.2,[63] and 5.3.2,[42] respectively. The morphologically examined active layers were prepared from the same batch as the examined OSC devices. GIWAXS data were obtained at an X-ray energy of 10 KeV and an incident angle of 0.2° (above the substrate critical angle), enabling intensities linear to the illuminated sample volume. Samples were spin-coated on Na/PSS/Si. In addition to the grazing incidence angle (0.2°), a rocking scan was acquired around an incident angle of 10.55, which is the specular angle of the pi−pi scattering peak of the polymer. Additional angles of incidence were explored as well (e.g., 5.18, 7.72, and 9.94°). The data at 7.72° were used to patch up the missing wedge in the 0.2° data and to analyze for pole figures in a similar fashion to previous literature by Toney et al.[64] RSoXS data were obtained at an X-ray energy below the C-edge at 283.5 eV. Samples were spin-coated on Na/PSS/Si substrates and then floated off in deionized water onto Si_3N4 windows, low-stress Si_3N4 membranes with a size of 2 mm^2 and a thickness of 100 nm. RSoXS data were normalized to film thickness, which was measured via NEXAFS spectra acquired at the same position as where RSoXS measurements were acquired and with the same X-ray beam. The RSoXS measurements were conducted in a transmission mode at normal incidence and also at 45 degrees of sample tilt (see Figure S22).

STXM images, to quantify chemical composition, were acquired at a fullerene resonant energy of 284.4 eV and a nonresonant energy of 320 eV. These energies were selected from NEXAFS spectra for neat materials. All STXM and NEXAFS samples were spin-coated on Na/PSS/Si substrates and then floated off in deionized water onto TEM grids.

■ ASSOCIATED CONTENT

Supporting Information

The Supporting Information is available free of charge at https://pubs.acs.org/doi/10.1021/acsami.1c15570.

> Detailed calculations of the D−A interfaces, more in-depth analysis of the X-ray measurements, and images of the RPV and bias-assisted charge extraction data (PDF)

■ AUTHOR INFORMATION

Corresponding Author

Brian A. Collins − *Materials Science and Engineering Program and Department of Physics and Astronomy, Washington State University, Pullman, Washington 99164, United States;* orcid.org/0000-0003-2047-8418; Email: brian.collins@wsu.edu

Authors

Obaid Alqahtani − *Materials Science and Engineering Program, Washington State University, Pullman, Washington 99164, United States; Department of Physics, Prince Sattam Bin Abdulaziz University, Alkharj 11942, KSA*

Seyed Mehrdad Hosseini − *Optoelectronics of Organic Semiconductors Institute, University of Potsdam, Potsdam-Golm 14476, Germany;* orcid.org/0000-0001-6981-115X

Thomas Ferron − *Department of Physics and Astronomy, Washington State University, Pullman, Washington 99164, United States*

Victor Murcia − *Materials Science and Engineering Program, Washington State University, Pullman, Washington 99164, United States*

Terry McAfee − *Department of Physics and Astronomy, Washington State University, Pullman, Washington 99164, United States; Advanced Light Source, Lawrence Berkeley National Laboratory, Berkeley, California 94720, United States*

Kevin Vixie − *Department of Mathematics, Washington State University, Pullman, Washington 99164, United States*

Fei Huang − *Institute of Polymer Optoelectronic Materials and Devices, State Key Laboratory of Luminescent Materials and Devices, South China University of Technology, Guangzhou 510640, P. R. China;* orcid.org/0000-0001-9665-6642

Ardalan Armin − *Department of Physics, Swansea University, Swansea, Wales SA2 8PP, U.K.;* orcid.org/0000-0002-6129-5354

Safa Shoaee − *Optoelectronics of Organic Semiconductors Institute, University of Potsdam, Potsdam-Golm 14476, Germany;* orcid.org/0000-0001-5754-834X

Complete contact information is available at: https://pubs.acs.org/10.1021/acsami.1c15570

Notes

The authors declare no competing financial interest.

■ ACKNOWLEDGMENTS

Major funding for this work was provided by the US National Science Foundation DMR Electronic and Photonics Program under grant #1905790 which also provided funding support for O.A. and T.M. The authors also acknowledge the Alexander von Humboldt Foundation (Sofja Kovalevskaja prize) for funding and Dieter Neher (PWM) for access to labs. Funding support for T.F. and V.M. was provided by the US Department of Energy Early Career Research Program under Grant DE-SC0017923. This research used resources of the Advanced Light Source, which is a DOE Office of Science User Facility under contract no. DE-AC02-05CH11231.

■ REFERENCES

(1) Scharber, M. C.; Sariciftci, N. S. Efficiency of Bulk-Heterojunction Organic Solar Cells. *Prog. Polym. Sci.* **2013**, *38*, 1929−1940.

(2) Liang, Y.; Feng, D.; Wu, Y.; Tsai, S.-T.; Li, G.; Ray, C.; Yu, L. Highly Efficient Solar Cell Polymers Developed via Fine-Tuning of Structural and Electronic Properties. *J. Am. Chem. Soc.* **2009**, *131*, 7792−7799.

(3) Meng, L.; Zhang, Y.; Wan, X.; Li, C.; Zhang, X.; Wang, Y.; Ke, X.; Xiao, Z.; Ding, L.; Xia, R.; Yip, H. L.; Cao, Y.; Chen, Y. Organic and Solution-Processed Tandem Solar Cells with 17.3% Efficiency. *Science* **2018**, *361*, 1094−1098.

(4) Liu, Q.; Jiang, Y.; Jin, K.; Qin, J.; Xu, J.; Li, W.; Xiong, J.; Liu, J.; Xiao, Z.; Sun, K.; Yang, S.; Zhang, X.; Ding, L. 18% Efficiency Organic Solar Cells. *Sci. Bull.* **2020**, *65*, 272−275.

(5) Neher, D.; Kniepert, J.; Elimelech, A.; Koster, L. J. A. A New Figure of Merit for Organic Solar Cells with Transport-Limited Photocurrents. *Sci. Rep.* **2016**, *6*, 24861.

(6) Bartesaghi, D.; Pérez, I. d. C.; Kniepert, J.; Roland, S.; Turbiez, M.; Neher, D.; Koster, L. J. A. Competition between Recombination and Extraction of Free Charges Determines the Fill Factor of Organic Solar Cells. *Nat. Commun.* **2015**, *6*, 7083.

(7) Armin, A.; Chen, Z.; Jin, Y.; Zhang, K.; Huang, F.; Shoaee, S. Shockley-Type Polymer: Fullerene Solar Cell. *Adv. Energy Mater.* **2018**, *8*, 1701450.

(8) Duan, C.; Gao, K.; Colberts, F. J. M.; Liu, F.; Meskers, S. C. J.; Wienk, M. M.; Janssen, R. A. J. Thiophene Rings Improve the Device Performance of Conjugated Polymers in Polymer Solar Cells with Thick Active Layers. *Adv. Energy Mater.* **2017**, *7*, 1700519.

(9) Shoaee, S.; Armin, A.; Stolterfoht, M.; Hosseini, S. M.; Kurpiers, J.; Neher, D. Decoding Charge Recombination through Charge Generation in Organic Solar Cells. *Sol. RRL* **2019**, *3*, 1900184.

(10) Gao, J.; Wang, J.; Xu, C.; Hu, Z.; Ma, X.; Zhang, X.; Niu, L.; Zhang, J.; Zhang, F. A Critical Review on Efficient Thick-Film Organic Solar Cells. *Sol. RRL* **2020**, *4*, 2000364.

(11) Andersen, T. R.; Dam, H. F.; Hösel, M.; Helgesen, M.; Carlé, J. E.; Larsen-Olsen, T. T.; Gevorgyan, S. A.; Andreasen, J. W.; Adams, J.; Li, N.; Machui, F.; Spyropoulos, G. D.; Ameri, T.; Lemaître, N.; Legros, M.; Scheel, A.; Gaiser, D.; Kreul, K.; Berny, S.; Lozman, O. R.; Nordman, S.; Välimäki, M.; Vilkman, M.; Søndergaard, R. R.; Jørgensen, M.; Brabec, C. J.; Krebs, F. C. Scalable, Ambient Atmosphere Roll-to-Roll Manufacture of Encapsulated Large Area, Flexible Organic Tandem Solar Cell Modules. *Energy Environ. Sci.* **2014**, *7*, 2925.

(12) Chang, Y.; Zhu, X.; Lu, K.; Wei, Z. Progress and Prospects of Thick-Film Organic Solar Cells. *J. Mater. Chem. A* **2021**, *9*, 3125−3150.

(13) Jin, Y.; Chen, Z.; Dong, S.; Zheng, N.; Ying, L.; Jiang, X. F.; Liu, F.; Huang, F.; Cao, Y. A Novel Naphtho[1,2- c :5,6- C′]Bis([1,2,5]Thiadiazole)-Based Narrow-Bandgap π-Conjugated Polymer with Power Conversion Efficiency Over 10. *Adv. Mater.* **2016**, *28*, 9811−9818.

(14) Langevin, P. Recombinaison et Mobilites Des Ions Dans Les Gaz. *Ann. Chim. Phys.* **1903**, *28*, 433−530.

(15) Ko, S.-J.; Walker, B.; Nguyen, T. L.; Choi, H.; Seifter, J.; Uddin, M. A.; Kim, T.; Kim, S.; Heo, J.; Kim, G.-H.; Cho, S.; Heeger, A. J.; Woo, H. Y.; Kim, J. Y. Photocurrent Extraction Efficiency near Unity in a Thick Polymer Bulk Heterojunction. *Adv. Funct. Mater.* **2016**, *26*, 3324−3330.

(16) Hosseini, S. M.; Tokmoldin, N.; Lee, Y. W.; Zou, Y.; Woo, H. Y.; Neher, D.; Shoaee, S. Putting Order into PM6:Y6 Solar Cells to Reduce the Langevin Recombination in 400 Nm Thick Junction. *Sol. RRL* **2020**, *4*, 2000498.

(17) Hosseini, S. M.; Roland, S.; Kurpiers, J.; Chen, Z.; Zhang, K.; Huang, F.; Armin, A.; Neher, D.; Shoaee, S. Impact of Bimolecular Recombination on the Fill Factor of Fullerene and Nonfullerene-Based Solar Cells: A Comparative Study of Charge Generation and Extraction. *J. Phys. Chem. C* **2019**, *123*, 6823−6830.

(18) Phuong, L. Q.; Hosseini, S. M.; Koh, C. W.; Woo, H. Y.; Shoaee, S. Measuring Competing Recombination Losses in a Significantly Reduced Langevin System by Steady-State Photoinduced Absorption and Photocurrent Spectroscopy. *J. Phys. Chem. C* **2019**, *123*, 27417−27422.

(19) Schwarz, K. N.; Geraghty, P. B.; Mitchell, V. D.; Khan, S.-U. -Z.; Sandberg, O. J.; Zarrabi, N.; Kudisch, B.; Subbiah, J.; Smith, T. A.; Rand, B. P.; Armin, A.; Scholes, G. D.; Jones, D. J.; Ghiggino, K. P. Reduced Recombination and Capacitor-like Charge Buildup in an Organic Heterojunction. *J. Am. Chem. Soc.* **2020**, *142*, 2562−2571.

(20) Murthy, D. H. K.; Melianas, A.; Tang, Z.; Juška, G.; Arlauskas, K.; Zhang, F.; Siebbeles, L. D. A.; Inganäs, O.; Savenije, T. J. Origin of Reduced Bimolecular Recombination in Blends of Conjugated Polymers and Fullerenes. *Adv. Funct. Mater.* **2013**, *23*, 4262−4268.

(21) Pivrikas, A.; Sariciftci, N. S.; Juška, G.; Österbacka, R. A Review of Charge Transport and Recombination in Polymer/Fullerene Organic Solar Cells. *Prog. Photovoltaics Res. Appl.* **2007**, *15*, 677−696.

(22) Ye, L.; Hu, H.; Ghasemi, M.; Wang, T.; Collins, B. A.; Kim, J.-H.; Jiang, K.; Carpenter, J. H.; Li, H.; Li, Z.; McAfee, T.; Zhao, J.; Chen, X.; Lai, J. L. Y.; Ma, T.; Bredas, J.-L.; Yan, H.; Ade, H. Quantitative Relations between Interaction Parameter, Miscibility and Function in Organic Solar Cells. *Nat. Mater.* **2018**, *17*, 253−260.

(23) Yan, H.; Swaraj, S.; Wang, C.; Hwang, I.; Greenham, N. C.; Groves, C.; Ade, H.; McNeill, C. R. Influence of Annealing and Interfacial Roughness on the Performance of Bilayer Donor/Acceptor Polymer Photovoltaic Devices. *Adv. Funct. Mater.* **2010**, *20*, 4329−4337.

(24) Lyons, B. P.; Clarke, N.; Groves, C. The Relative Importance of Domain Size, Domain Purity and Domain Interfaces to the Performance of Bulk-Heterojunction Organic Photovoltaics. *Energy Environ. Sci.* **2012**, *5*, 7657.

(25) Zimmerman, J. D.; Xiao, X.; Renshaw, C. K.; Wang, S.; Diev, V. V.; Thompson, M. E.; Forrest, S. R. Independent Control of Bulk and Interfacial Morphologies of Small Molecular Weight Organic Heterojunction Solar Cells. *Nano Lett.* **2012**, *12*, 4366−4371.

(26) McMahon, D. P.; Cheung, D. L.; Troisi, A. Why Holes and Electrons Separate So Well in Polymer/Fullerene Photovoltaic Cells. *J. Phys. Chem. Lett.* **2011**, *2*, 2737−2741.

(27) Clarke, T. M.; Rodovsky, D. B.; Herzing, A. A.; Peet, J.; Dennler, G.; DeLongchamp, D.; Lungenschmied, C.; Mozer, A. J. Significantly Reduced Bimolecular Recombination in a Novel Silole-Based Polymer: Fullerene Blend. *Adv. Energy Mater.* **2011**, *1*, 1062−1067.

(28) Collins, B. A.; Li, Z.; Tumbleston, J. R.; Gann, E.; McNeill, C. R.; Ade, H. Absolute Measurement of Domain Composition and Nanoscale Size Distribution Explains Performance in PTB7:PC71BM Solar Cells. *Adv. Energy Mater.* **2013**, *3*, 65−74.

(29) Alqahtani, O.; Babics, M.; Gorenflot, J.; Savikhin, V.; Ferron, T.; Balawi, A. H.; Paulke, A.; Kan, Z.; Pope, M.; Clulow, A. J.; Wolf, J.; Burn, P. L.; Gentle, I. R.; Neher, D.; Toney, M. F.; Laquai, F.; Beaujuge, P. M.; Collins, B. A. Mixed Domains Enhance Charge Generation and Extraction in Bulk-Heterojunction Solar Cells with Small-Molecule Donors. *Adv. Energy Mater.* **2018**, *8*, 1702941.

(30) Ferron, T.; Waldrip, M.; Pope, M.; Collins, B. A. Increased Charge Transfer State Separation via Reduced Mixed Phase Interface in Polymer Solar Cells. *J. Mater. Chem. A* **2019**, *7*, 4536−4548.

(31) Dhakal, P.; Ferron, T.; Alotaibi, A.; Murcia, V.; Alqahtani, O.; Collins, B. A. Evidence for Field-Dependent Charge Separation Caused by Mixed Phases in Polymer−Fullerene Organic Solar Cells. *J. Phys. Chem. Lett.* **2021**, *12*, 1847.

(32) Venkatesan, S.; Chen, J.; Ngo, E. C.; Dubey, A.; Khatiwada, D.; Zhang, C.; Qiao, Q. Critical Role of Domain Crystallinity, Domain Purity and Domain Interface Sharpness for Reduced Bimolecular Recombination in Polymer Solar Cells. *Nano Energy* **2015**, *12*, 457−467.

(33) Ye, L.; Zhang, S.; Ma, W.; Fan, B.; Guo, X.; Huang, Y.; Ade, H.; Hou, J. From Binary to Ternary Solvent: Morphology Fine-Tuning of D/A Blends in PDPP3T-Based Polymer Solar Cells. *Adv. Mater.* **2012**, *24*, 6335−6341.

(34) Vandewal, K.; Gadisa, A.; Oosterbaan, W. D.; Bertho, S.; Banishoeib, F.; Van Severen, I.; Lutsen, L.; Cleij, T. J.; Vanderzande, D.; Manca, J. V. The Relation Between Open-Circuit Voltage and the Onset of Photocurrent Generation by Charge-Transfer Absorption in Polymer : Fullerene Bulk Heterojunction Solar Cells: Photocurrent Generation by Charge-Transfer Absorption. *Adv. Funct. Mater.* **2008**, *18*, 2064−2070.

(35) Stolterfoht, M.; Armin, A.; Shoaee, S.; Kassal, I.; Burn, P.; Meredith, P. Slower Carriers Limit Charge Generation in Organic Semiconductor Light-Harvesting Systems. *Nat. Commun.* **2016**, *7*, 11944.

(36) Armin, A.; Juska, G.; Ullah, M.; Velusamy, M.; Burn, P. L.; Meredith, P.; Pivrikas, A. Balanced Carrier Mobilities: Not a Necessary Condition for High-Efficiency Thin Organic Solar Cells as Determined by MIS-CELIV. *Adv. Energy Mater.* **2014**, *4*, 1300954.

(37) Zhang, K.; Chen, Z.; Armin, A.; Dong, S.; Xia, R.; Yip, H.-L.; Shoaee, S.; Huang, F.; Cao, Y. Efficient Large Area Organic Solar Cells Processed by Blade-Coating With Single-Component Green Solvent. *Sol. RRL* **2018**, *2*, 1700169.

(38) Armin, A.; Subbiah, J.; Stolterfoht, M.; Shoaee, S.; Xiao, Z.; Lu, S.; Jones, D. J.; Meredith, P. Reduced Recombination in High Efficiency Molecular Nematic Liquid Crystalline: Fullerene Solar Cells. *Adv. Energy Mater.* **2016**, *6*, 1600939.

(39) Rivnay, J.; Mannsfeld, S. C. B.; Miller, C. E.; Salleo, A.; Toney, M. F. Quantitative Determination of Organic Semiconductor Microstructure from the Molecular to Device Scale. *Chem. Rev.* **2012**, *112*, 5488−5519.

(40) Richter, L. J.; DeLongchamp, D. M.; Amassian, A. Morphology Development in Solution-Processed Functional Organic Blend Films: An In Situ Viewpoint. *Chem. Rev.* **2017**, *117*, 6332−6366.

(41) Li, Z.; Jiang, K.; Yang, G.; Lai, J. Y. L.; Ma, T.; Zhao, J.; Ma, W.; Yan, H. Donor Polymer Design Enables Efficient Non-Fullerene Organic Solar Cells. *Nat. Commun.* **2016**, *7*, 13094.

(42) Kilcoyne, A. L. D.; Tyliszczak, T.; Steele, W. F.; Fakra, S.; Hitchcock, P.; Franck, K.; Anderson, E.; Harteneck, B.; Rightor, E. G.; Mitchell, G. E.; Hitchcock, A. P.; Yang, L.; Warwick, T.; Ade, H. Interferometer-Controlled Scanning Transmission X-Ray Microscopes at the Advanced Light Source. *J. Synchrotron Radiat.* **2003**, *10*, 125−136.

(43) Collins, B. A.; Ade, H. Quantitative Compositional Analysis of Organic Thin Films Using Transmission NEXAFS Spectroscopy in an X-Ray Microscope. *J. Electron Spectrosc. Relat. Phenom.* **2012**, *185*, 119−128.

(44) Collins, B. A.; Gann, E. Resonant Soft X-Ray Scattering in Polymer Science. *J. Polym. Sci.* **2021**, *1*, 1−45.

(45) Tumbleston, J. R.; Collins, B. A.; Yang, L.; Stuart, A. C.; Gann, E.; Ma, W.; You, W.; Ade, H. The Influence of Molecular Orientation on Organic Bulk Heterojunction Solar Cells. *Nat. Photonics* **2014**, *8*, 385−391.

(46) Ferron, T.; Pope, M.; Collins, B. A. Spectral Analysis for Resonant Soft X-Ray Scattering Enables Measurement of Interfacial Width in 3D Organic Nanostructures. *Phys. Rev. Lett.* **2017**, *119*, 167801.

(47) Kozub, D. R.; Vakhshouri, K.; Orme, L. M.; Wang, C.; Hexemer, A.; Gomez, E. D. Polymer Crystallization of Partially Miscible Polythiophene/Fullerene Mixtures Controls Morphology. *Macromolecules* **2011**, *44*, 5722−5726.

(48) Pfannmöller, M.; Flügge, H.; Benner, G.; Wacker, I.; Sommer, C.; Hanselmann, M.; Schmale, S.; Schmidt, H.; Hamprecht, F. A.; Rabe, T.; Kowalsky, W.; Schröder, R. R. Visualizing a Homogeneous Blend in Bulk Heterojunction Polymer Solar Cells by Analytical Electron Microscopy. *Nano Lett.* **2011**, *11*, 3099−3107.

(49) Guo, C.; Kozub, D. R.; Kesava, S. V.; Wang, C.; Hexemer, A.; Gomez, E. D. Signatures of Multiphase Formation in the Active Layer of Organic Solar Cells from Resonant Soft X-Ray Scattering. *ACS Macro Lett.* **2013**, *2*, 185−189.

(50) Mukherjee, S.; Proctor, C. M.; Tumbleston, J. R.; Bazan, G. C.; Nguyen, T.-Q.; Ade, H. Importance of Domain Purity and Molecular Packing in Efficient Solution-Processed Small-Molecule Solar Cells. *Adv. Mater.* **2015**, *27*, 1105−1111.

(51) Albrecht, S.; Schindler, W.; Kurpiers, J.; Kniepert, J.; Blakesley, J. C.; Dumsch, I.; Allard, S.; Fostiropoulos, K.; Scherf, U.; Neher, D. On the Field Dependence of Free Charge Carrier Generation and Recombination in Blends of PCPDTBT/PC $_{70}$ BM: Influence of Solvent Additives. *J. Phys. Chem. Lett.* **2012**, *3*, 640−645.

(52) Venkatesan, S.; Adhikari, N.; Chen, J.; Ngo, E. C.; Dubey, A.; Galipeau, D. W.; Qiao, Q. Interplay of Nanoscale Domain Purity and Size on Charge Transport and Recombination Dynamics in Polymer Solar Cells. *Nanoscale* **2014**, *6*, 1011−1019.

(53) Erb, T.; Zhokhavets, U.; Gobsch, G.; Raleva, S.; Stühn, B.; Schilinsky, P.; Waldauf, C.; Brabec, C. J. Correlation Between Structural and Optical Properties of Composite Polymer/Fullerene Films for Organic Solar Cells. *Adv. Funct. Mater.* **2005**, *15*, 1193−1196.

(54) Solanki, A.; Wu, B.; Salim, T.; Lam, Y. M.; Sum, T. C. Correlation between Blend Morphology and Recombination Dynamics in Additive-Added P3HT:PCBM Solar Cells. *Phys. Chem. Chem. Phys.* **2015**, *17*, 26111−26120.

(55) Vohra, V.; Kawashima, K.; Kakara, T.; Koganezawa, T.; Osaka, I.; Takimiya, K.; Murata, H. Efficient Inverted Polymer Solar Cells Employing Favourable Molecular Orientation. *Nat. Photonics* **2015**, *9*, 403−408.

(56) Jamieson, F. C.; Domingo, E. B.; McCarthy-Ward, T.; Heeney, M.; Stingelin, N.; Durrant, J. R. Fullerenecrystallisation as a Key Driver of Charge Separation in Polymer/Fullerene Bulk Heterojunction Solar Cells. *Chem. Sci.* **2012**, *3*, 485−492.

(57) Szmytkowski, J. On the Tendency of Temperature and Electric Field Dependences of Interface Recombination in a P3HT:PCBM Organic Bulk Heterojunction Solar Cell. *Semicond. Sci. Technol.* **2011**, *26*, 105012.

(58) Gorenflot, J.; Heiber, M. C.; Baumann, A.; Lorrmann, J.; Gunz, M.; Kämpgen, A.; Dyakonov, V.; Deibel, C. Nongeminate Recombination in Neat P3HT and P3HT:PCBM Blend Films. *J. Appl. Phys.* **2014**, *115*, 144502.

(59) Awartani, O.; Lemanski, B. I.; Ro, H. W.; Richter, L. J.; DeLongchamp, D. M.; O'Connor, B. T. Correlating Stiffness, Ductility, and Morphology of Polymer:Fullerene Films for Solar Cell Applications. *Adv. Energy Mater.* **2013**, *3*, 399−406.

(60) Do, K.; Huang, D. M.; Faller, R.; Moulé, A. J. A Comparative MD Study of the Local Structure of Polymer Semiconductors P3HT and PBTTT. *Phys. Chem. Chem. Phys.* **2010**, *12*, 14735.

(61) Feng, S.; Zhang, C. e.; Liu, Y.; Bi, Z.; Zhang, Z.; Xu, X.; Ma, W.; Bo, Z. Fused-Ring Acceptors with Asymmetric Side Chains for High-Performance Thick-Film Organic Solar Cells. *Adv. Mater.* **2017**, *29*, 1703527.

(62) Hexemer, A.; Bras, W.; Glossinger, J.; Schaible, E.; Gann, E.; Kirian, R.; MacDowell, A.; Church, M.; Rude, B.; Padmore, H. A SAXS/WAXS/GISAXS Beamline with Multilayer Monochromator. *J. Phys.: Conf. Ser.* **2010**, *247*, 012007.

(63) Gann, E.; Young, A. T.; Collins, B. A.; Yan, H.; Nasiatka, J.; Padmore, H. A.; Ade, H.; Hexemer, A.; Wang, C. Soft X-Ray Scattering Facility at the Advanced Light Source with Real-Time Data Processing and Analysis. *Rev. Sci. Instrum.* **2012**, *83*, 045110.

(64) Baker, J. L.; Jimison, L. H.; Mannsfeld, S.; Volkman, S.; Yin, S.; Subramanian, V.; Salleo, A.; Alivisatos, A. P.; Toney, M. F. Quantification of Thin Film Crystallographic Orientation Using X-Ray Diffraction with an Area Detector. *Langmuir* **2010**, *26*, 9146−9151.

https://doi.org/10.1021/acsami.1c15570